ID 166

Drag Analysis for an Economic Helicopter

S. Schneider, S. Mores, M. Edelmann, A. D'Alascio, D. Schimke
Aerodynamics
Eurocopter Deutschland GmbH
81663 Munich, Germany
e-mail: sascha.schneider@eurocopter.com

In view of a growing ecological awareness in society the economic thought gains in increasingly significance at EUROCOPTER. The current paper focuses therefore on a detailed investigation of the drag fractions of several components of the EC135 helicopter and is divided into three sections. The first section reports on the validation of numerical predictions by means of CFD against wind tunnel measurements about the EC135 wind tunnel model. The measurements are being carried out at the Technical University of Munich between winter 2010 and spring 2011. The second section relates the drag breakdown over several components of the full-scale EC135 helicopter only by means of CFD simulations. For this purpose, several configurations with different level of complexity will be investigated. Dependent on the complexity of the considered configuration both the multi-block structured (U)RANS solver FLOWer and the edge based unstructured (U)RANS solver TAU, each developed at DLR, will be applied. Finally the paper concludes with an outlook toward an economic helicopter by disclosing the potential of aerodynamic improvements of selected components.

INTRODUCTION

In recent years a growing ecological awareness in society is perceived, which motivates industry to invest more and more attention and funding towards the development of "blue" or "green" concepts. EUROCOPTER following the year 2020 goals of ACARE (Advisory Council for Aeronautics Research in Europe) is highly motivated to work towards an efficient and economic helicopter. One of the key elements of the economic helicopter is the improvement of the aerodynamic efficiency, i.e. reducing the direct and interference drag of several components of the helicopter.

Therefore, a thorough understanding of the flow phenomena and interference effects around several components of the helicopter is essential to improve its aerodynamic characteristics. Experimental investigations of the complex and unsteady flow field around helicopters, either by wind tunnel experiments or flight tests, usually provide information on global loads only rather than a detailed view of the flow structure, unless elaborate unsteady measurements of the flow field and analysis of the unsteady pressure on the helicopter are carried out. In contrast Computational Fluid Dynamics (CFD) is established as a research and development tool in helicopter industry and enables a more detailed investigation of the three-dimensional aerodynamic flow phenomena and interference effects during the design process.

NUMERICAL APPROACH

Code Description

Dependent on the complexity of the considered configuration the numerical investigations in this paper are performed with both the multi-block structured (U)RANS solver FLOWer and the edge based unstructured (U)RANS solver TAU, each developed at DLR. General information about the codes are given in [1], [2] and [3] as regards to FLOWer and in [4] and [5] concerning the TAU code.

TAU:

The TAU code solves the (U)RANS equations on unstructured grids and facilitates the four primary element types: tetrahedra, hexahedra, prisms and pyramids. The spatial discretization is based on a cell-vertex finite volume formulation using the dual grid, which is computed during a pre-processing step. Central differences along with matrix artificial dissipation have also been used for the convective fluxes and low velocities are accounted for by a pre-conditioning technique. TAU offers a wide range of turbulence models, ranging from simple algebraic ones, 1- and 2-transport equation models to full RSM models. All TAU simulations described in this paper made use of the 2-transport equation Menter-SST model. The convective fluxes of turbulence equations are discretized with the Roe or the AUSMDV scheme. The time derivative is also discretized using implicit backward Euler

differences and the discrete equation system is integrated by an implicit LU scheme. Convergence acceleration is implemented by local time stepping, residual smoothing and a multigrid method. Finally, greater flexibility for complex simulations is ensured through wrapping Python classes that allow direct addressing of the main subroutines of TAU.

FLOWer:

The flow solver FLOWer solves the compressible three-dimensional (U)RANS equations on structured multiblock grids. The spatial discretization, based on a cell-centred finite volume formulation, makes use of central differences along with scalar artificial dissipation. The time discretization is implemented with backward Euler differences and integration is carried out through a 5-stage Runge-Kutta scheme. For accelerating the convergence local time stepping, implicit residual smoothing and the multigrid method are applied. Turbulence effects can be accounted for by a series of algebraic, 1 or 2-transport equation or even Reynolds-stress transport (RSM) models. In this paper the 2-equation Wilcox k-ω is applied to the respective FLOWer simulations.

Validation of numerical predictions against wind tunnel

This first section reports on the validation of numerical simulations by means of CFD against wind tunnel measurements, which are being carried out at the Technical University of Munich between winter 2010 and spring 2011. The experimental investigation is performed in open test section mode and the scaled model is equipped with about 128 steady pressure ports, 15 unsteady Kulites placed on the backdoor and the upper rear part of the engine fairing and finally 6 unsteady Kulites on the vertical fin.

Since the measurement campaign at the University of Munich is still ongoing, presently only a comparison of the global loads is possible. A detailed analysis of the unsteady pressure data and the PIV data will follow.

Model geometry

Figure 1 shows a close view of the EC135 wind tunnel configuration (scale 1:7.3). Within the experimental setup the inlet and outlet of the engine compartment and the Fenestron have been closed. The model geometry for the numerical simulations corresponds to the experimental model, which was used prior to the wind tunnel tests. However, there is a difference between both geometries. The numerical computations are presently carried out without the rotor head, whereas the measurements are performed with rotating rotor head. Furthermore the experimental model is connected to a support strut whereas the CFD model only possesses the first element of the support strut. Figure 1 and Figure 2 show the experimental and the CFD model, respectively.

Figure 1: Wind tunnel model of the EC135

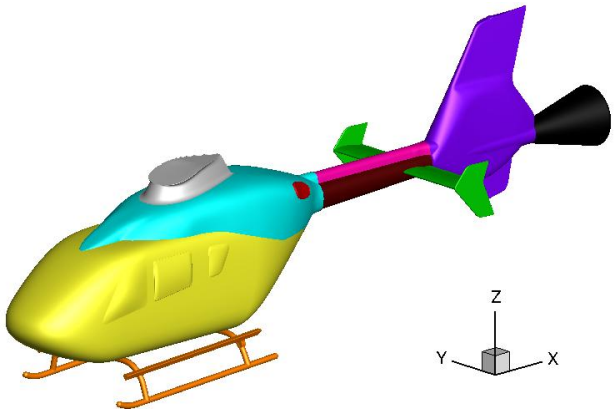

Figure 2: CFD model of the EC135

An overview of the components is given in Table 1.

Component	Colour
landing skid	orange
cabin	yellow
pylon	magenta
mast fairing	grey
exhausts	red
drive shaft	pink
tail boom	brown
horizontal stabilizer & end plates	green
fin & shroud & bumper	purple
support strut	black

Table 1: List of components

Case description

All numerical computations have been performed with the TAU code in steady and unsteady mode (steady: 20000 iterations / unsteady: 400 time steps with 200 sub iterations). Therefore five different test cases have been analysed at constant angle of attack and different yaw angles**.** Table 2 lists the initial conditions and test cases.

M_∞	0.178	[-]
p_∞	94465	[Pa]
T_∞	284.85	[K]
q_∞	2107.72	[Pa]
ρ_∞	1.1555	[kg/m³]
Δt	$0.23*10^{-3}$	[s]
Menter-SST	steady / unsteady	[-]
angle of attack	0	[°]
yaw angle	-20 / -10 / 0 / 10 / 20	[°]

Table 2: Initial conditions and test cases

Grid system

The underlying grid system has been generated by means of the commercial software ICEM-Tetra, see ref. [8]. It is a hybrid mesh which consists of 27 prism layers (green) around the solid surfaces, necessary to model the boundary layer flow correctly. The remaining volume extended to the far field is filled-up with tetrahedra (black). Prisms and tetrahedra are connected with the aid of pyramids. Figure 3 depicts the hybrid grid of the EC135 wind tunnel model.

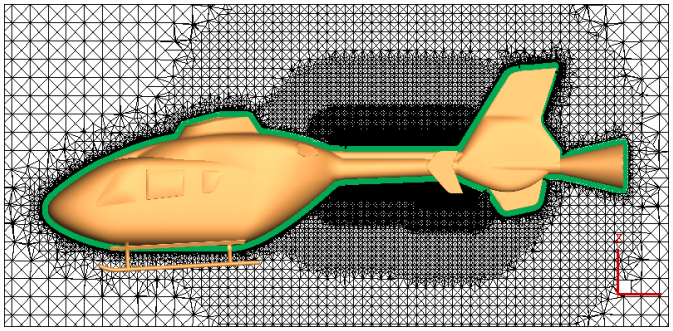

Figure 3: Hybrid mesh of EC135 wind tunnel model

Comparison of numerical and experimental results

Figure 4 and Figure 5 show a comparison of the numerical and experimental determined force and moment coefficients. The solid lines with round data points represent the measured data, whereas the computational results are applied with rectangular data points. All coefficients are shown in the wind frame coordinate system. The drag coefficient is marked with red colour, side force coefficients with green colour and lift force coefficients with blue colour. The numerical results, presented in this report, have been gained by averaging the computed force and moment coefficients over the last 200 time steps of the unsteady run.

All computed coefficients show a good correlation with the experimental data. According to the force coefficients of Figure 4 the discrepancy between the computational and experimental data is due to the different model geometry. The rotor head of the wind tunnel model exerts a higher drag and lift force which causes the almost constant discrepancy of the experimental and numerical data concerning the lift and drag force coefficient.

As for the force coefficients the moment coefficients also show good accordance of computed and experimental data. The biggest deviation of data lies at a yaw angle of +/- 20°. Again the aberration between computational and experimental data is due to the different model geometry.

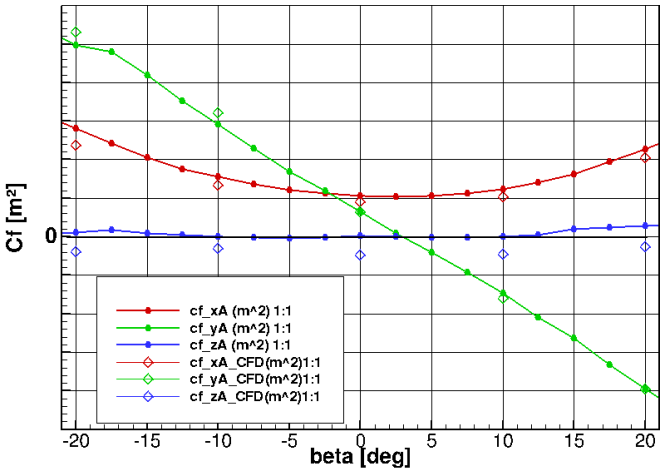

Figure 4: Force coefficients

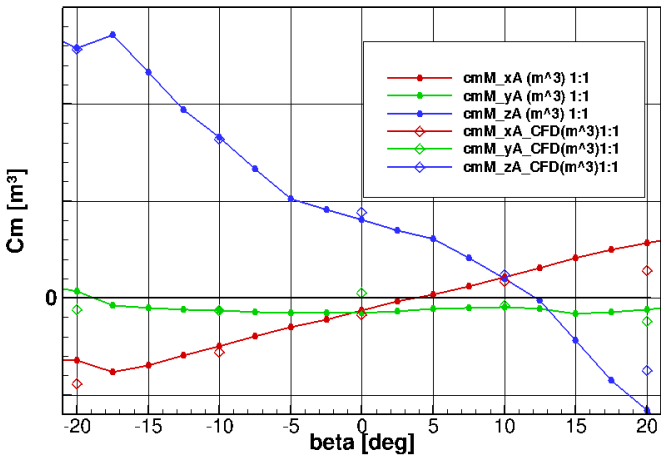

Figure 5: Moment coefficients

Drag breakdown over several components of the full-scale EC135 helicopter

This section relates the drag breakdown over several components of the full-scale EC135 helicopter only by means of CFD simulations. For this purpose, several configurations with different level of complexity will be investigated.

Configurations

The analysis of the drag starts with the isolated fuselage of the EC135 with closed Fenestron® duct and closed engine inlets and exhausts. The basic geometry setup is shown in Figure 6.

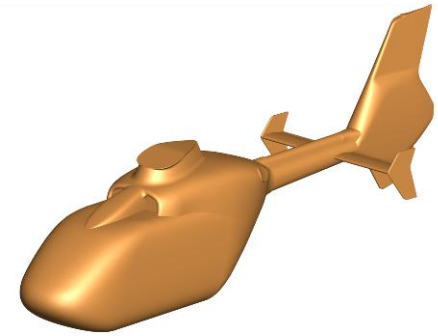

Figure 6: Configuration 1 - Isolated fuselage with closed Fenestron® duct and engine inlet and exhaust

The next level of complexity is defined by adding the landing skid components (green colored components indicated in Figure 7) consisting of the two landing skids, the front and rear bending tubes and the left and right step.

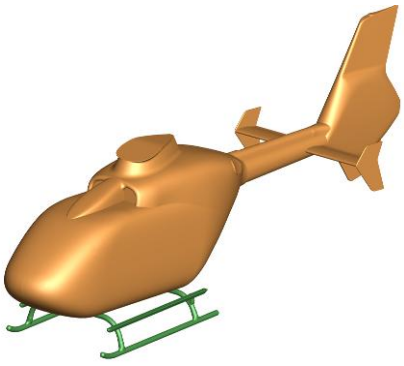

Figure 7: Configuration 2 - Based on configuration 1 including landing skid components

Replacing the Navier-Stokes boundary condition by an engine boundary condition enables the simulation of an air mass flow through the inlet of the engine fairing and out of the engine exhaust (Figure 8). Additionally the high temperature of the exhaust gases can be simulated by setting a temperature ratio at the engine exhaust boundary.

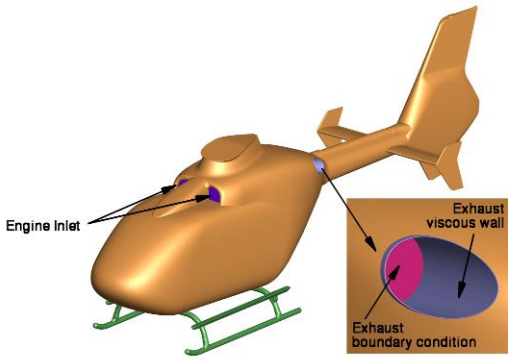

Figure 8: Configuration 3 - Additionally simulation of air mass flow through the inlet of the engine fairing and out of the engine exhaust

As indicated in Figure 9, the next level of complexity is defined by introducing an actuator disc for determining the influence of the main rotor on the fuselage. The loads distribution of the actuator disc for the corresponding flight state is provided by the in-house tool HOST. The TAU code can directly read in the loads file of HOST using the implemented interface.

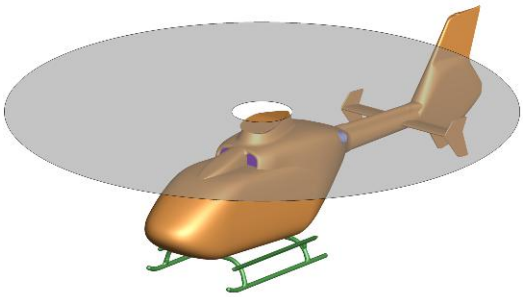

Figure 9: Configuration 4 – Additionally simulation of the influence of the main rotor on the fuselage by using an actuator disc approach

Finally, the configuration with the highest level of complexity includes components of the engine deck, for instance the oil cooler, the rotor and Fenestron® shaft, the gearbox and the engine inlets, and components of the Fenestron®, for instance the stator blades, the Fenestron® gearbox and the drive shaft fairing. Both the main rotor and the Fenestron® rotor are simulated by means of an actuator disc. Additionally, the floor of the cabin, as well as the assembly of the landing skid and the fuselage is modelled more realistically.

Moreover the convex windows are integrated in the fuselage. All modifications of the geometry are illustrated in Figure 10.

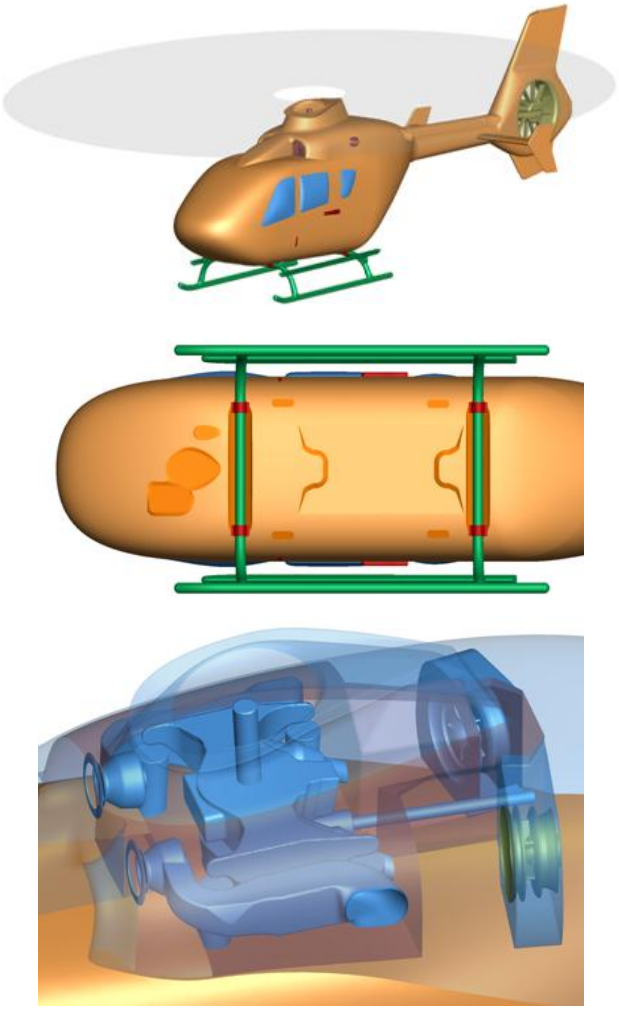

Figure 10: Configuration 5 - Highest level of complexity

Mesh generation

The structured grids are generated with the HEXA module of the commercial grid generator ICEMCFD and are based on a structured multi-block approach. As the structured mesh generation of complex geometries is very sophisticated, only the first three configurations will be considered for comparison of the results between FLOWer and TAU. Additionally a different meshing strategy is necessary for constructing the structured grids. The landing skid components and engine exhaust components are embedded in several sub-grids communicating with the fuselage mesh through Chimera interpolations. Figure 11 and Figure 12 illustrate the integration of the several Chimera component grids into the complete grid system. The global grid system of configuration 2 includes in total five Chimera component meshes whereas the global grid system of configuration 3 includes overall seven Chimera sub-grids.

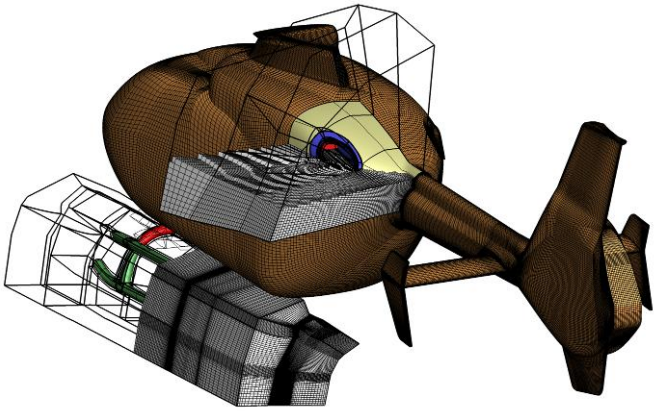

Figure 11: Structured sub-grids of configuration 3

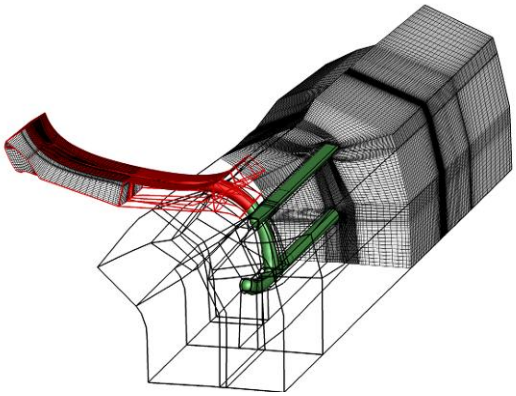

Figure 12: Mesh of landing skid (green) and front landing skid conncetor (red)

An overview of the mesh sizes of the different structured sub-grids are presented in Table 3.

Configuration	Part	Blocks	Cells [Mio.]
1	**Complete**	**135**	**8.270**
2	Fuselage	135	8.383
	LandingSkid (LK) (right)	48	2.037
	LandingSkid (LK) (left)	48	2.037
	LK-Connector (front)	24	0.274
	LK-Connector (rear)	24	0.240
	Complete	**279**	**12.971**

3	Fuselage	135	8.383
	LandingSkid (LK) (right)	48	2.037
	LandingSkid (LK) (left)	48	2.037
	LK-Connector (front)	24	0.274
	LK-Connector (rear)	24	0.240
	Engine Exhaust (right)	18	0.274
	Engine Exhaust (left)	18	0.240
	Complete	**315**	**12.971**

Table 3: Structured grid statistic

The unstructured grids for the flow solver TAU have been prepared with the commercial software CENTAUR of CentaurSoft. The hybrid meshing technique using the four primarily element types (tetrahedra, hexahedra, prisms and pyramids) enables the generation of a one block mesh without the need of applying the Chimera method. Structured hexahedra elements mainly used on the stator blades, the horizontal stabiliser, the backdoor and the landing skids facilitate higher stretching ratio of the cells and therefore a reduction of mesh points. Additionally the grid and solution quality is improved.

Figure 13 presents exemplarily parts of the surface mesh, whereas Figure 14 shows exemplarily a cut through the volume mesh at the position y=0.

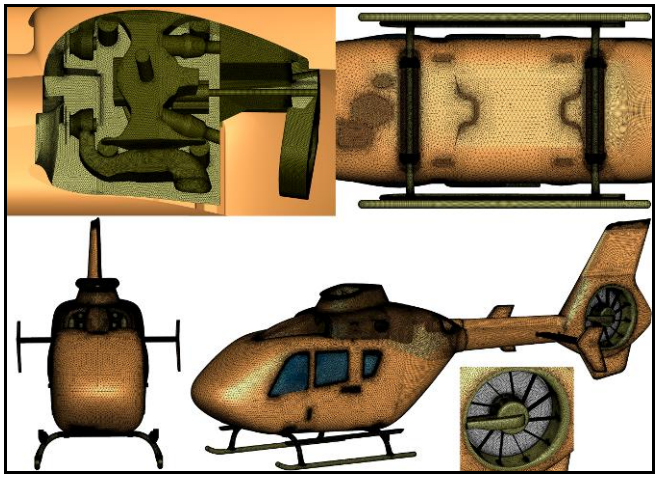

Figure 13: Surface mesh generated by CENTAUR

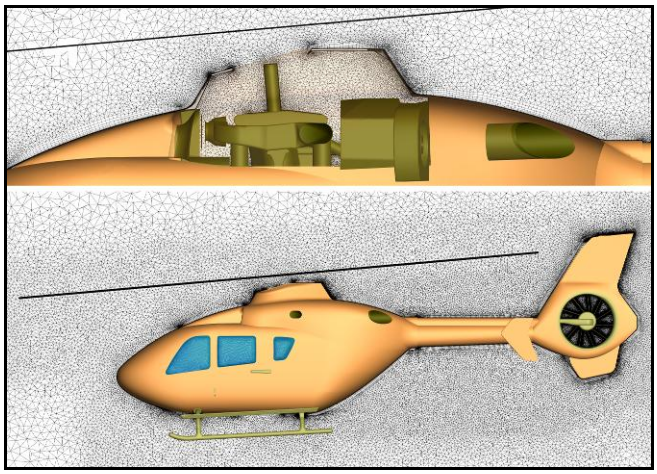

Figure 14: Cut through volume mesh at position y=0

Table 4 summarizes the unstructured grid statistic for the respective configuration.

Configuration	Blocks	Points
1	**1**	**5377118**
2	**1**	**7926226**
3	**1**	**11276581**
4	**1**	**11045683**
5	**1**	**32975146**

Table 4: Unstructured grid statistic

Case description

The considered flight state for the drag analysis is defined as a fast level flight at a true air speed of 140kts and an altitude of 5000ft (ISA condition). The helicopter pitch angle for all configurations is set to -1.5° whereas the side slip angle for configuration 1 and 2 is defined as -1.5° and changes to 0.0° for configuration 3 to 5. Table 5 summarizes the flight conditions.

Altitude and atmospheric condition	5000ft ISA
True Air Speed (TAS)	140kts
Helicopter pitch angle	-1.5°
Helicopter side slip angle (Configuration 1 and 2)	-1.5°
Helicopter side slip angle (Configuration 3, 4 and 5)	0.0°

Table 5: Flight conditions

Discussion of the numerical results

The results of the drag analysis are presented in Figure 15. For this purpose the total drag is divided into three parts: the drag of the fuselage components, the tailboom components and the landing skid components. The shaded colored bars of Figure 15 belong to the corresponding FLOWer computation whereas the solid colored bars representing the TAU computations.

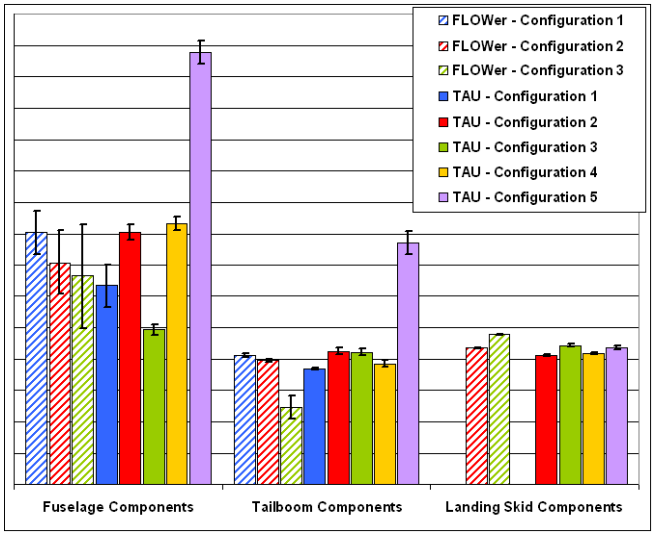

Figure 15: EC135 – drag breakdown

The drag analysis of the landing skid components results in a good correlation between the several configurations as well as the different applied flow solvers. Moreover the low RMS deviations, indicated by the black error bars, suggest converged drag values. Regarding the drag of the tailboom components a massive drag increase of configuration 5 is noticed. This drastic drag increase can be explained with the additional Fenestron® components integrated in the complete configuration and the flow separation in the front part of the Fenestron® duct, shown in Figure 16.

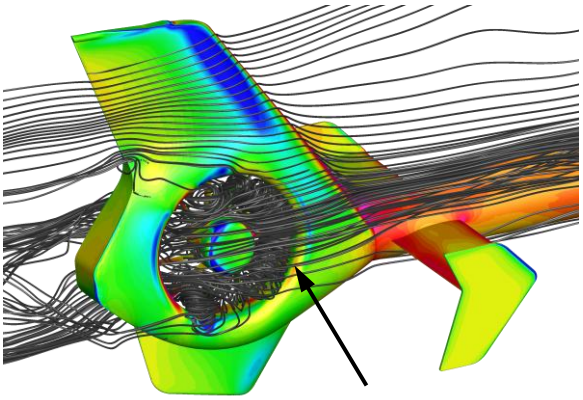

Figure 16: Flow separation in the Fenestron duct

The flow separation occurs since the Fenestron rotor, represented by an actuator disc, produces only sparse thrust in the fast level flight condition. Except for configuration 3 (simulated with the FLOWer code) the drag values of the tailboom components also show a good correlation between the different configurations and the different flow solvers. The value of configuration 3 seems not to be fully converged since the error bars of both the drag of the fuselage components and the tailboom components show a wider bandwidth compared to the other drag values. The results of the predicted drag of the fuselage components show the largest dispersion between the different configurations and flow solvers. First starting with configuration 5 the increased drag can be explained again by the additional components of the engine deck and the associated change of the unsteady flow field in and around the engine deck indicated in Figure 17.

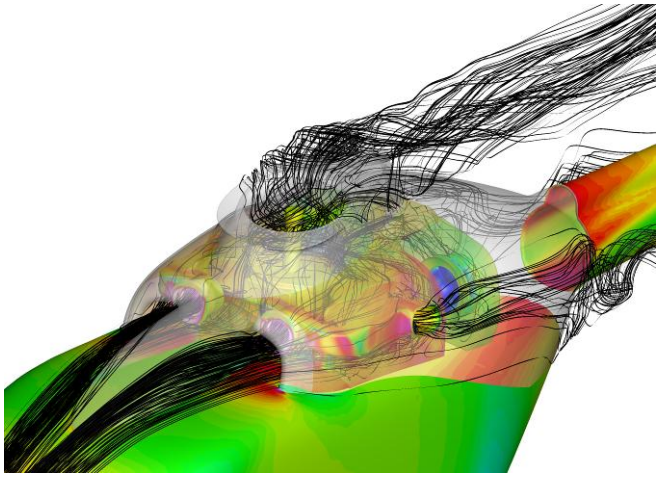

Figure 17: Unsteady flow field in and around the engine deck

Moreover the integration of the windows, the floor of the cabin and the assembly of the landing skid components and the fuselage also affects the unsteady flow field and accounts for the drag increase. Introducing the landing skid components influence not only the flow field at the floor of the cabin but also the flow field and the flow separation position at the backdoor. Figure 18 demonstrates a snap-shot of the different cp distributions and streamtraces of the cabin floor and the backdoor for the configurations 1, 3 and 5 (TAU code). The landing skid components influence massively the flow field and the streamtraces at the backdoor. Compared to the baseline configuration the flow field behind the rear cross tube possess an intense unsteady character and the flow separation occurs more upstream. With the detailed floor of configuration 5 there

is no continuous flow from the helicopter nose to the flange of the tailboom. At each bending tube the flow is interrupted which results in a completely different flow behaviour at the backdoor. In the snap-shot of Figure 18 there is a reverse flow beginning at the flange of the tailboom and going upstream to the rear cross tube.

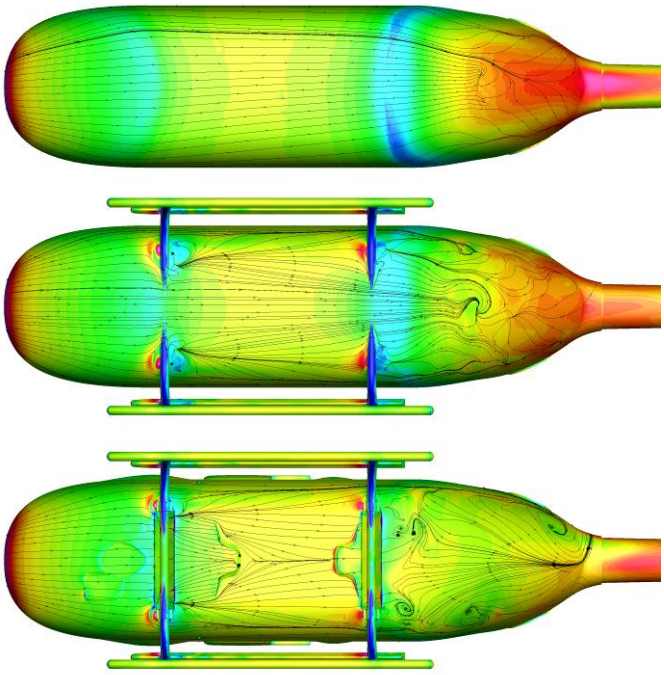

Figure 18: Flow field at the floor of the cabin and at the backdoor

General speaking the flow field at the cabin floor and backdoor is characterized as turbulent and unsteady and is very sensitive which also arises in larger RMS deviations of the drag and the apparently contrary behaviour of the drag values between the configurations and between FLOWer and TAU. The reduction of the drag between configuration 1 or 2 and 3 can be qualitatively explained by the different flow situation at the inlet of the engine deck. In configuration 1 and 2 the inlet of the engine deck is closed and a retention effect of the air is formed. This turbulent and unsteady air generates a vortex going downstream along the edge between the fuselage and the engine deck. Setting the engine boundary condition and simulating an air mass flow through the inlet of the engine fairing reduces this effect and therefore the drag. The quantitative amount of drag reduction however seems to be too large and cannot be explained presently. Indicated in Figure 19 the assumed value for the mass flow is too small since the retention effect still can be observed. Only when the simulating the complete engine deck the retention effect vanishes.

Introducing the main rotor represented by an actuator disc increases the drag mainly of the fuselage components. The downwash effect of the main rotor even in fast level flight slightly changes the flow field around the engine deck and therefore also the flow field of the remaining fuselage components are affected.

Concluding it can be summarized that the flow field around a helicopter is inherent unsteady and for this reason an unsteady numerical simulation is necessary. The drag prediction especially of the backdoor remains difficult due to the flow separation occurring with this kind of configuration. Previous studies showed an influence on the results dependent on the chosen turbulence model and the mesh quality.

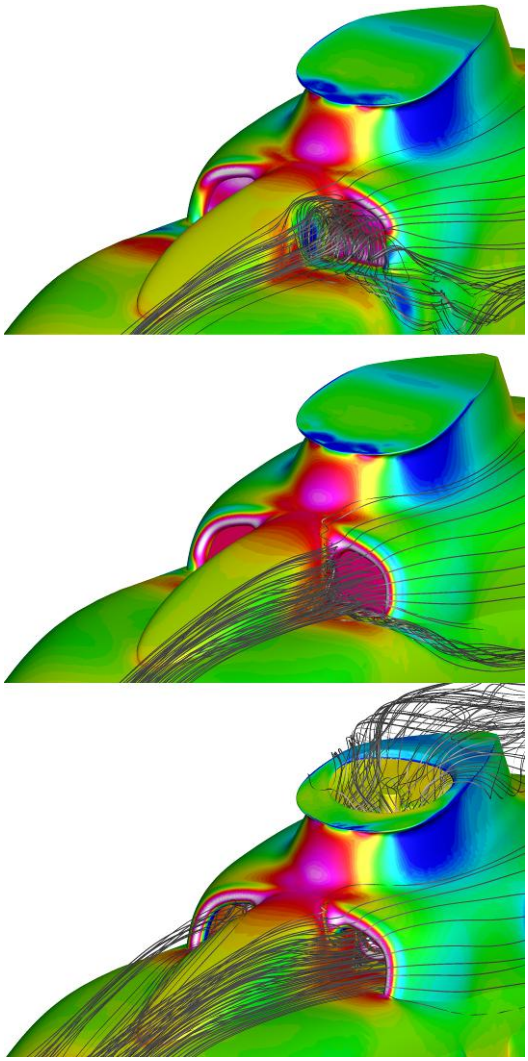

Figure 19: Different flow situation at the inlet of the engine deck between the different configurations

Optimisation of fuselage components

This last section will give an outlook towards an economic helicopter by disclosing the potential of aerodynamic improvements of selected components. For this purpose a study of passive shape modifications on the lightweight class helicopter EC135 was conducted within the frame of the development of environmental compatible helicopters, Green Rotor Craft (GRC). Detailed aerodynamic investigations were carried out with main emphasis on the drag reduction. Main focus was on the modification of the landing gear and the aft body region, which were identified as the main drag contributors. In the following investigation no passive means, such as strakes or vortex generators, were applied to influence the airflow around the backdoor. Additionally there was no constraint of the download force of the fuselage given, since flight mechanic investigations have shown little effect on the helicopter performance due to the download effects. However reducing the download of the fuselage would be favourable.

Case description

Since the drag reduction process has to be represented by a typical flight situation, a fast level flight at the true air speed of 140kts and an altitude of 5000ft in ISA conditions was selected for this analysis. Both the rotor head and the components of the Fenestron anti-torque system were not considered in the CFD computation. However each of the four computations includes an engine boundary condition to represent a more realistic airstream around the aft region of the fuselage. Table 6 summarizes the setup of the simulations.

Altitude and atmospheric condition	5000ft ISA
True Air Speed (TAS)	140kts (72m/s)
Helicopter pitch angle	-1.5deg
Helicopter yaw/roll angle	0.0deg

Table 6: Optimisation of fuselage components: computational setup

Configurations

In the context of the fuselage optimisation investigation three modified backdoors were investigated to determine the aerodynamic drag improvements. Based on the serial EC135 baseline configuration the three improved configurations have faired landing skids. The baseline configuration and the three modified configurations are described in the following. The several components of the baseline configuration shown in Figure 20 are abstracted into the following main parts: Fuselage, Tail Unit and Landing Gear

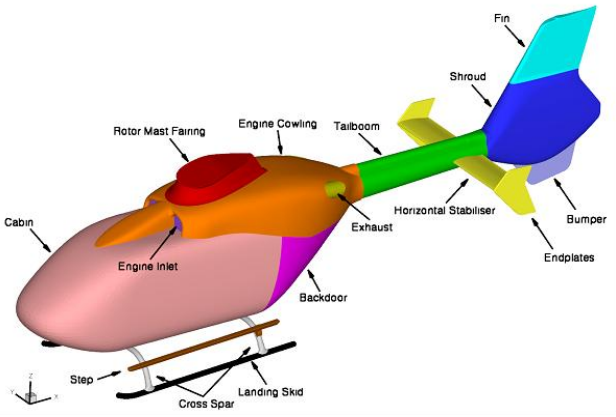

Figure 20: Baseline - EC135

The improved configurations A to C which are described in the following paragraph comprise faired cross tubes (Figure 21) to reduce both the overall and the component drag. The fairing is not limited to the cross tubes, additionally the mountings (clamps) to the fuselage and the floor of the cabin are faired as well. The cross-section of the tube fairings are described by a laminar airfoil which is trimmed to produce minimal drag (hence minimal lift) in the specified flight condition described in this report. Important to mention is that the front cross tube fairings in general tend to reduce the overall dynamic stability which must be considered in flight mechanics. Moreover the left and right step between the front and rear bending / cross tubes of the following configurations are integrated into the new fairings of the cross tubes.

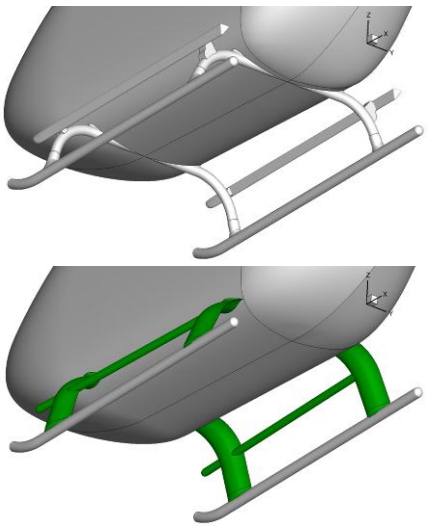

Figure 21: Faired cross tubes (the modified cross tubes and steps are marked green)

Configuration A is illustrated in Figure 22 and contains a modified backdoor which closes in a sharp edge at the rear end of the backdoor section and therefore representing a sharp trailing edge. Compared to the baseline configuration the area of separation is reduced due to the reduced curvature of the backdoor splines.

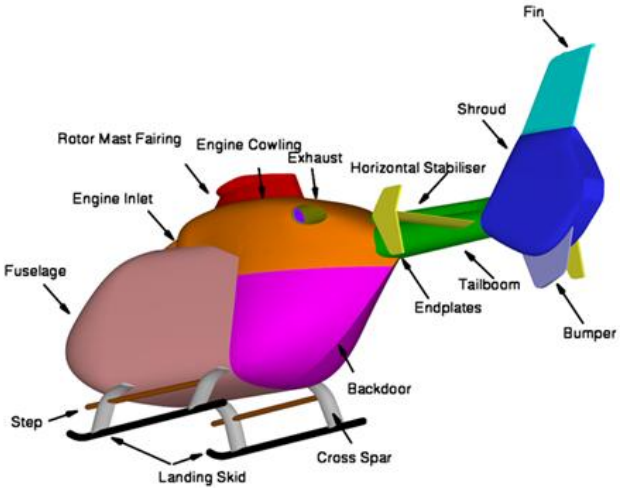

Figure 22: Configuration A – sharp trailing edge closing the backdoor

Configuration B shown in Figure 23 contains the identical backdoor as seen from configuration A, however the sharp trailing edge is truncated at the aft region to reduce the extension of the surface. The truncation is located aft of the flow separation region to minimize increasing drag.

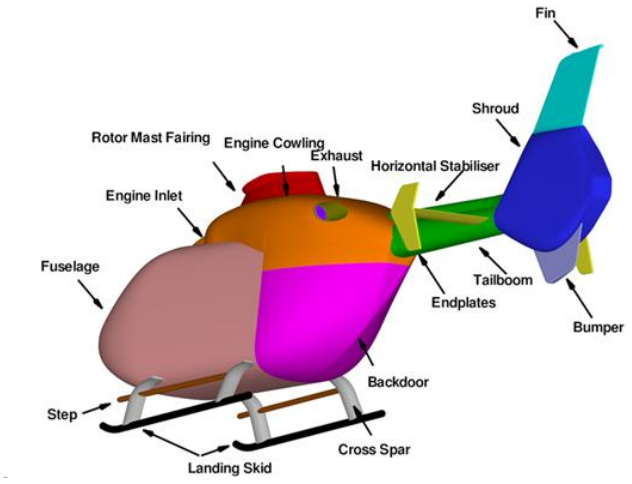

Figure 23: Configuration B – truncated sharp trailing edge closing the backdoor

The last investigated configuration C (Figure 24) contains a backdoor with defined flow separation edges at the junction between the bottom and side surface of the backdoor. These edges should separate the flow into two regions: the bottom flow and the side airflow.

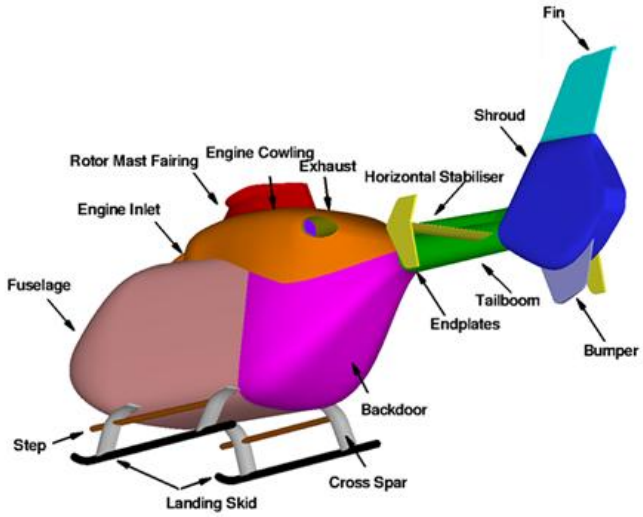

Figure 24: Configuration C – backdoor with defined flow separation edges

Grid System

All unstructured meshes for this study were generated using the grid generator CENTAUR of CentaurSoft. Several components, for instance the step, the landing gear fairing, the tailboom and the horizontal stabilisers were meshed with structured elements to improve the grid quality, solution quality and to reduce overall grid size. The mesh sizes range from 9 to 11 Million nodes.

Discussion of the numerical results

The computations are carried out with the TAU code using the Menter SST turbulence model.

Drag breakdown

Figure 25 shows the drag breakdown of all three modified configurations, relatively to the baseline configuration. In general it can be said, that the modification of the backdoor and adding a cross tube fairing an overall drag reduction benefit of approximately ~24% can be reached. As can be seen, the main drag reduction contributors are the landing skids and the backdoor. Since the flow around the backdoor is changed significantly due to the reshaped backdoors, faired cross tubes as well as removing floor roughness, the tail unit is affected slightly negatively due to an increased dynamic pressure resulting from the separated vortices. This effect will be described in the following chapter.

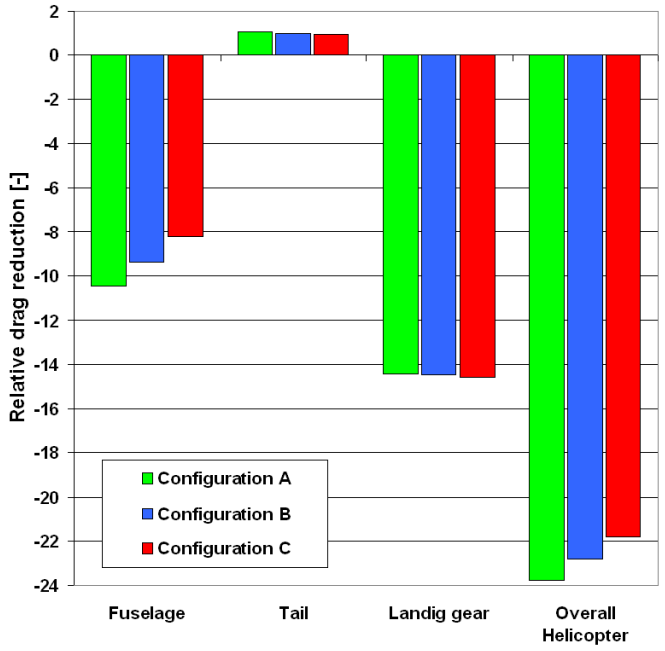

Figure 25: Relative drag breakdown of the main components

Due to the implementation of faired cross tubes all three modified configurations show a reduction of the fuselage drag. This results due to the cleaned floor as well as due to less flow separation resulting from the junction between cross tubes and fuselage. Configuration C has the least drag reduction improvement on the fuselage itself, which is a result of the reshaped engine compartment which had to be modified, since it is connected to the backdoor. This configuration is the only configuration which already includes constraints from the department for mechanical engineering, thus the constraints leads to the above mentioned higher drag of the compartment. For the future development the area of engine compartment may be an area which will need further improvement studies.

Since this shown breakdown only represents one flight condition, computing a flight envelope may be needed to gain further potential of drag reduction of all components.

Pressure contour & surface streamlines

The following figures deal with the flow on the surface of the EC135 baseline and the three modifications. For this Figure 26 to Figure 29 show the pressure coefficient and the streamlines on the surface of the helicopter.

Viewing on the streamlines it is clearly visible that the separation line on the backdoor's side is shifted in a further aft position which reduces the overall separation surface on the entire backdoor (marked with the red 1 in the figures). This reduces the separation region on the backdoor which leads to beneficial drag values.

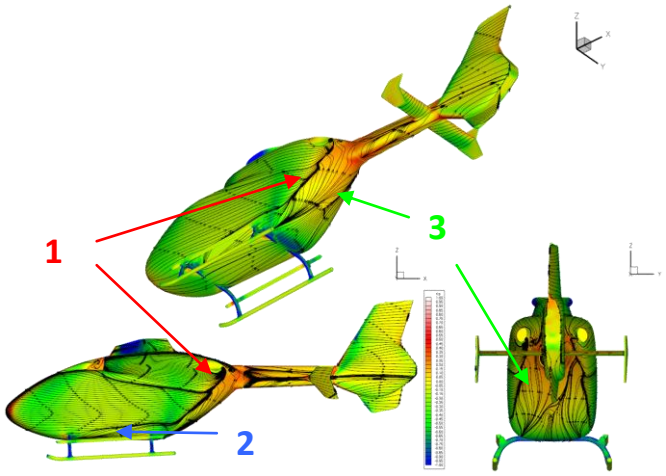

Figure 26: EC135 Baseline - Pressure coefficient contour & surface streamlines

The modified design of the junction between fuselage and cross tube at the front and rear shows that less flow separation occurs in this specific area which affects the backdoor flow (marked with the blue 2 in the figures) positively. Without this reshaped junction, as in the baseline configuration, the separation affects the backdoor region negatively. This effect shows that if the backdoor shall be modified to improve drag, the cross tubes or anything else in front of the backdoor may influencing the stream negatively must be removed or modified.

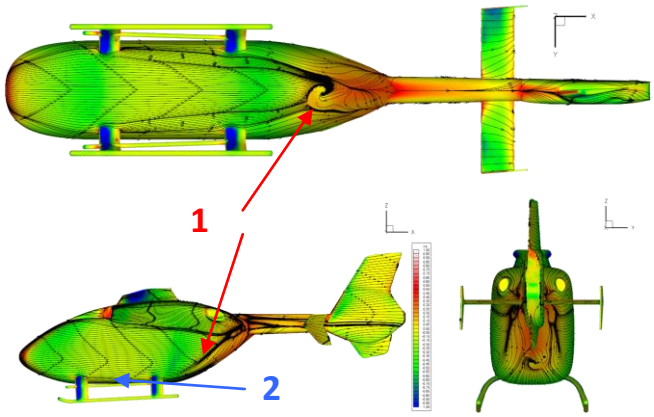

Figure 27: Configuration A - Pressure coefficient contour & surface streamlines

All three modified backdoor have an obviously changed pressure region compared to the baseline configuration.

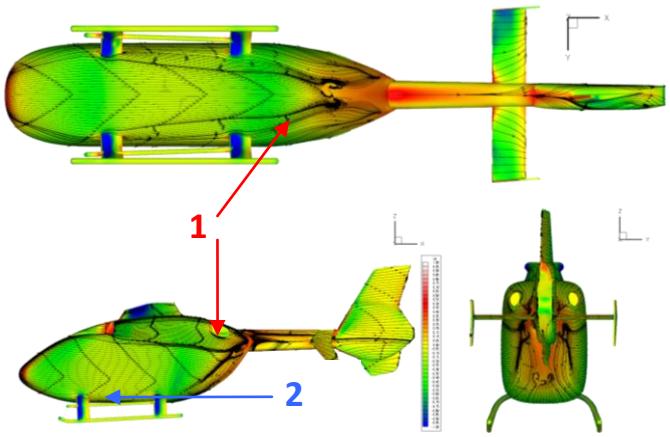

Figure 28: Configuration B - Pressure coefficient contour & surface streamlines

The pressure region of all three configurations shows an area of higher pressure which reduces drag of the backdoor due to less suction effects. This is a result of the distinctive flow separation regions on the backdoors.

As in Figure 26 the flow on the backdoor has an arbitrary flow pattern which results from the mixing of the flow from the fuselage side and bottom. Configuration C (Figure 29) shows a clear separation between the sideway and the bottom flow which seems to be influencing the drag beneficial (marked with a green 3 in the figures).

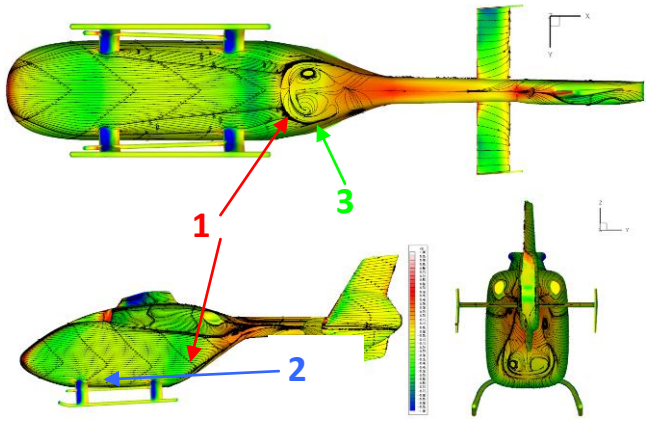

Figure 29: Configuration C - Pressure coefficient contour & surface streamlines

Kinematic vorticity

The following figures show the volume flow around the backdoors of the EC135 baseline and the three modifications. For this Figure 30 to Figure 33 show multiple kinematic vorticity slices in the aft region to visualize the strength of the vortices separating from the helicopter surface.

The effect of the implemented cross tube fairing and junction between fuselage and cross tubes is clearly visible when comparing the baseline (Figure 30) with the modified configurations (Figure 31 to Figure 33) (marked with a black 4 in the figures). Due to the fairings the kinematic vorticity in the aft region is reduced significantly which has shown a drag benefit on the fuselage itself in Figure 31. Comparing the baseline (Figure 30) with configuration C (Figure 33) the defined edges on the backdoor produce so-called “round edge vortices” which lead to the already mentioned increased pressure region on the backdoor surface itself (marked with a black 5 in the figures), yet these also hit the empennage with higher dynamic pressure. This effect leads to slightly higher drag values of the empennage. Since this analysis represents only one specific flight condition it may be interesting to analyse this effect on the tail unit for a wider range of fuselage angle settings.

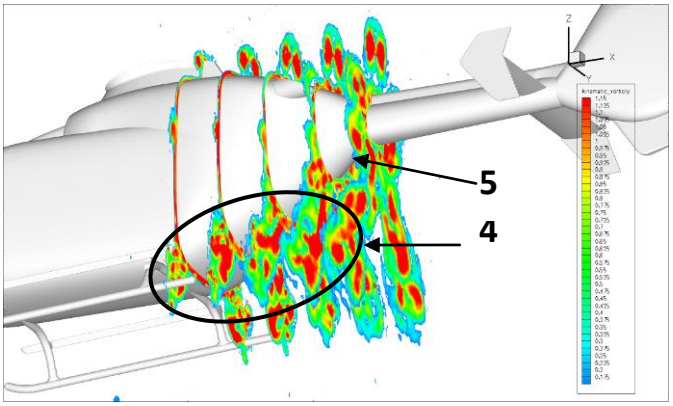

Figure 30: EC135 Baseline - Kinematic Vorticity

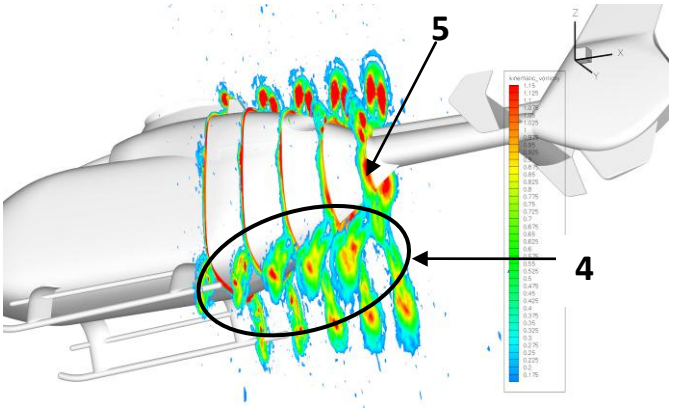

Figure 31: Configuration A - Kinematic Vorticity

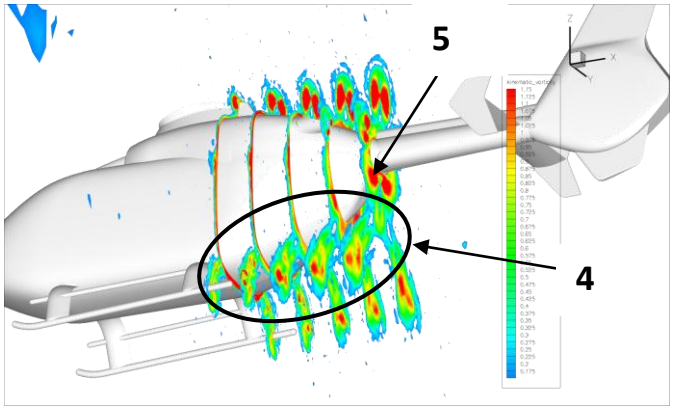

Figure 32: Configuration B - Kinematic Vorticity

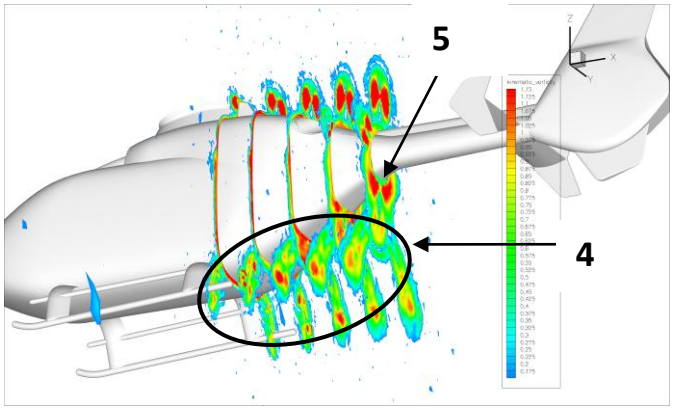

Figure 33: Configuration C - Kinematic Vorticity

CONCLUSION AND OUTLOOK

A first comparison of the loads between the solution of the numerical simulation and the experimental wind tunnel data generally shows a good correlation. Since the measurement campaign at the University of Munich is still ongoing, a detailed analysis of the unsteady pressure data and the PIV data will follow.

The analysis of the drag of the full-scale EC135 helicopter serves as first evaluation phase to determine the main contributors of the overall drag for the following optimization phase. Besides the drag of the rotor head, which was not part of the present investigation, the main contributors of the drag are indentified as the floor of the cabin, the backdoor and the landing skid components.

Therefore the last section concentrates on three modified backdoor configurations with faired cross tubes of the landing gear compared with the baseline configuration in order to reduce the overall helicopter drag. The results of the optimization show that all three configurations yield in a promising drag reduction potential. Moreover it has been shown that a backdoor with defined flow separation edges at the junction between the bottom and side surface of the backdoor split the airflow into two separated regions and leads to good drag benefits. However the results also show that the engine compartment may be reshaped in order to increase the drag benefit locally without neglecting the constructional constraints given for this configuration. The tail unit of all three configurations have increased drag values which result from higher dynamic pressure due to the changed flow pattern in the separation region of the backdoor. Since the study represents only one specific cruise condition it may be necessary to check further points of the flight envelope to confirm the determined drag benefit.

Concluding only the combination of an optimised backdoor with an optimised landing gear results in significant drag benefits.

ACKNOWLEDGEMENTS

The authors would like to thank the German ministry of Economy and Labour (BMWA) for its funding in the framework of ECO-HC (grant 20H0803).

REFERENCES

[1] Kroll, N., Eisfeld, B., and Bleecke, H.M. “The Navier-Stokes Code FLOWer”, volume 71 of Notes on Numerical Fluid Mechanics, pages 58-71. Vieweg, Braunschweig, 1999.

[2] Schwarz, T.: The Overlapping Grid Technique For The Time Accurate Simulation of Rotorcraft Flows. Proceedings of the 31st European Rotorcraft Forum, September 2005

[3] Kroll, N.; Rossow, C.-C.; Becker, K.; Thiele, F.: The MEGAFLOW Project. In: Aerospace Science and Technology, Vol. 4, 2002, pp. 223-237

[4] Gerhold, T.; Galle, M.; Friedrich, O.; Evans, J.: Calculation of Complex Three-Dimensional Configurations Employing The DLR TAU-Code. AIAA-97-0167, 1997.

[5] Schwamborn, D.; Gerhold, T.; Heinrich R.: The DLR Tau-code: Recent Applications In Research And Industry. In: Proceeding of ECCOMAS CFD 2006, Egmond aan Zee, Netherlands, September 5th-8th, 2006.

[6] Borie, S.; Mosca, J.; Sudre, L.; Benoit, C.; Péron, S.: Influence of Rotor Wakes On Helicopter

Aerodynamic Behaviour. In: Proceedings of the 35th European Rotorcraft Forum, Hamburg, Germany, September 22nd-25th, 2009.

[7] F. Le Chuiton, T. Kneisch, S. Schneider and Ph. Krämer “Industrial validation of numerical aerodynamics about rotor heads: towards a design optimisation at EUROCOPTER”, Proceedings of the 35th European Rotorcraft Forum, Hamburg, Germany, September 22nd-25th, 2009.

[8] N.N.: ICEM-CFD 4.2.2, User Manual 2003Kroll, N.; Rossow, C.-C.; Becker, K.; Thiele, F.: The MEGAFLOW Project. In: Aerospace Science and Technology, Vol. 4, 2002, pp. 223-237